TECHNICAL PAPER

Effect of tool materials on performance of rotary tool micro-USM process during fabrication of microchannels

Sandeep Kumar[1] · Akshay Dvivedi[1]

Abstract

The tool wear affects the efficiency of micro-USM process and the quality of machined micro-features. In this research endeavor, wear mechanism of soft/ductile and hard/brittle tool materials is investigated comprehensively. Stainless steel-304 (SS-304) and tungsten carbide (WC) were selected as tool materials for rotary tool micro-USM (RT-MUSM) process. The effect of tool material properties on tool wear and performance of RT-MUSM process is also discussed. The effect of RT-MUSM process parameters, viz. rotation speed, feed rate, power rating and slurry concentration on material removal rate (MRR), depth of channel (DOC) and width over cut (WOC) are reported. The experimental results showed that SS-304 tool worn out rapidly due to plastic deformation followed by strain hardening. The superior properties of WC such as high wear resistance, compressive strength and good acoustic property led to reduction in tool wear and thereby significantly improved the performance of RT-MUSM. Additionally, multi-response optimization was applied to obtain maximum MRR, DOC and minimum WOC simultaneously.

Keywords RT-MUSM · Tool material · MRR · DOC · WOC · Silica glass · Optimization

1 Introduction

The industrial applicability of electrically non-conductive materials (e.g., glass, quartz and silicon) is increasing exponentially in the applications such as microfluidics, bio-MEMS, micro heat exchanger, lab-on-chip devices, etc. [1–3]. Glass is preferable work material for the aforesaid applications due to its high corrosion resistance, wear resistance, chemical resistance, high strength and thermal resistance. However, owing to such superior properties, precision micromachining of glass using conventional machining methods is extremely difficult, costly and time consuming [4]. Therefore, to meet the demand for precision machining, the development of efficient and economic advanced micromachining techniques is essential. Nowadays,

micro-ultrasonic machining (micro-USM) is becoming popular for machining of micro-features in all kind of hard and brittle materials including glass, ceramics and quartz. It has the ability to machine both the electrically conductive as well as insulating materials [5]. In micro-USM, material removal takes place from the work surface by abrasion caused due to hammering/impact action followed by micro-chipping, cavitation and chemical action [6]. Unlike other non-traditional methods, such as micro-EDM, micro-ECM, ECDM and laser, the micro-USM process does not affect the metallurgical and mechanical properties of work material [7]. Micro-USM has proved its efficacy to machine complex shapes in all types of hard and brittle materials. Moreover, the assistance of ultrasonic energy enhances the performance of both conventional and non-conventional machining methods (i.e., turning, milling and drilling) during machining of difficult-to-cut high strength materials/alloys [8–17].

In micro-USM, the accuracy of the micro-feature entirely depends on the shape of the tool. Since, the shape of the tool replicates on the workpiece, even a slight change in the shape of the tool in the form of tool wear may lead to a completely defective product. Thus, to make dimensionally accurate micro-features, the first and foremost requirement is to maintain the shape and size of the tool (i.e., reduction

✉ Sandeep Kumar
  sandeepkumar71@gmail.com

  Akshay Dvivedi
  akshaydvivedi@gmail.com

1 Mechanical and Industrial Engineering Department, Indian Institute of Technology Roorkee, Roorkee 247667, India

in tool wear). Tool wear is an inevitable phenomenon of micro-USM and hence it is an important issue. According to the published literature, in micro-USM, tool wear is divided into three categories, i.e., longitudinal wear, lateral wear and edge rounding wear [18]. Longitudinal wear is reduction in tool length due to the hammering and cavitation phenomenon in between the tool, abrasives and work material. Lateral wear is taper formation in the vertical face of the tool due to the abrasion caused by moving abrasives in between the vertical face of the tool and wall of the machined cavity. Edge rounding wear is the reduction in diameter of the tool bottom face caused by the abrasion. In previous research work, some studies have been conducted to measure tool wear and its effect on the performance of micro-USM. Zuyuan et al. [19] proposed a theoretical model of tool wear to predict tool wear and revealed that low cycle fatigue is responsible for tool wear in micro-USM process. Jain et al. [20] proposed a new method called "Reference Point Method" to calculate the linear tool wear in micro-USM process. In their study, a hollow tool was compared with solid tool while drilling of silicon. They reported that hollow tool wears out faster than solid tool because of rapid work hardening caused by an increase in stresses due to lesser working area.

Micro-USM is a complex process in which tool wear depends on multiple process parameters (e.g., tool material properties, shape and size of abrasive, power rating, frequency, amplitude, etc.) with interaction effects on process outcomes. Among the various factors, the properties of tool material come under the most influencing parameters affecting micro-USM. Therefore, the selection of suitable tool material is very important in this process as far as efficiency and accuracy of machined micro-feature is concerned. In the earlier studies, thoriated tungsten, nimonic alloy, stainless steel (SS), tungsten carbide (WC), silver steel, high speed steel (HSS), titanium, mild steel, etc. have been used as tool materials in macro- and micro-USM process [19–22]. Komaraiah and Reddy [21] in their study on tool materials reported that tool material hardness influences both the longitudinal and lateral wear, whereas impact strength influences the lateral wear. Another investigation recommended the suitability of WC over SS-304 tool [23]. It is interesting to note that investigations by Wang et al. [24] prefer SS-304 over WC and 1045 carbon steel tools. They reported that 304 stainless steel tool has maximum material removal capability as compared to both the WC and 1045 carbon steel tool materials. Based on the above mentioned literature, it can be concluded that there are conflicting opinions regarding the selection of tool material in micro-USM process. Also, the wear mechanism of both the soft/ductile and hard/brittle tool material is also not clearly addressed in the published literature. Without revealing the wear mechanism of tool materials, the selection of suitable tool material for micro-USM process is very difficult.

Apart from tool materials, accumulation of debris into the gap between tool and workpiece (i.e., machining gap) is another issue which deteriorates the performance of micro-USM [25]. The poor circulation of abrasive slurry in the machining gap is responsible for debris accumulation. This results in severe tool wear and consequently low machining efficiency and poor form accuracy of machined micro-features. Kumar and Dvivedi [26] reported that the rotary motion of tool in micro-USM process overcome the problem of debris accumulation and improved the performance of micro-USM. Kumar and Dvivedi [27] revealed the mechanism of tool wear in RT-MUSM and reported that tool rotation in micro-USM process not only reduces the tool wear but also improves the accuracy of microchannels. Further, to enhance the geometrical capabilities as well as the efficiency of micro-USM process, there is still a need to explore the micro-USM process by selecting suitable tool material (i.e., soft/ductile or hard/brittle) on the basis of wear mechanism. To achieve this objective, tool wear mechanisms for both soft/ductile and hard/brittle need to be explored comprehensively. Furthermore, the efficiency of micro-USM process can also be enhanced by controlling and optimizing the input process parameters. Considering all the above mentioned issues, the present research paper reports on a comparative study on the effect of tool materials in the rotary tool micro-USM (RT-MUSM) process. The mechanisms of tool wear of both the soft/ductile and brittle material were discussed based on microscopic images. The effects of tool material properties on tool wear and performance of RT-MUSM process were also investigated. Later, the effect of RT-MUSM process parameters, viz. rotation speed, feed rate, power rating and slurry concentration on depth of channel (DOC), material removal rate (MRR) and width overcut (WOC) was investigated. Additionally, desirability-based multi-response optimization was employed to achieve maximum DOC, MRR and minimum WOC simultaneously.

2 Materials and methods

In this investigation, microchannels were fabricated on glass by adopting layer-by-layer machining approach [22, 27]. The glass is composed of silicon oxide (70%), boron oxide (11.5%), sodium oxide (9.5%), potassium oxide (7.5%) and barium oxide (1%) along with some foreign elements [28]. A self-developed RT-MUSM facility shown in Fig. 1 was used for experimentation in this study [29]. The RT-MUSM facility consists of power supply, rotary transducer unit, slurry feeding unit and XY table. The XY table was used to provide linear motion to the workpiece with a resolution of 0.1 μm. The movement to the table was given by a programming unit using software of 3-axis programmable
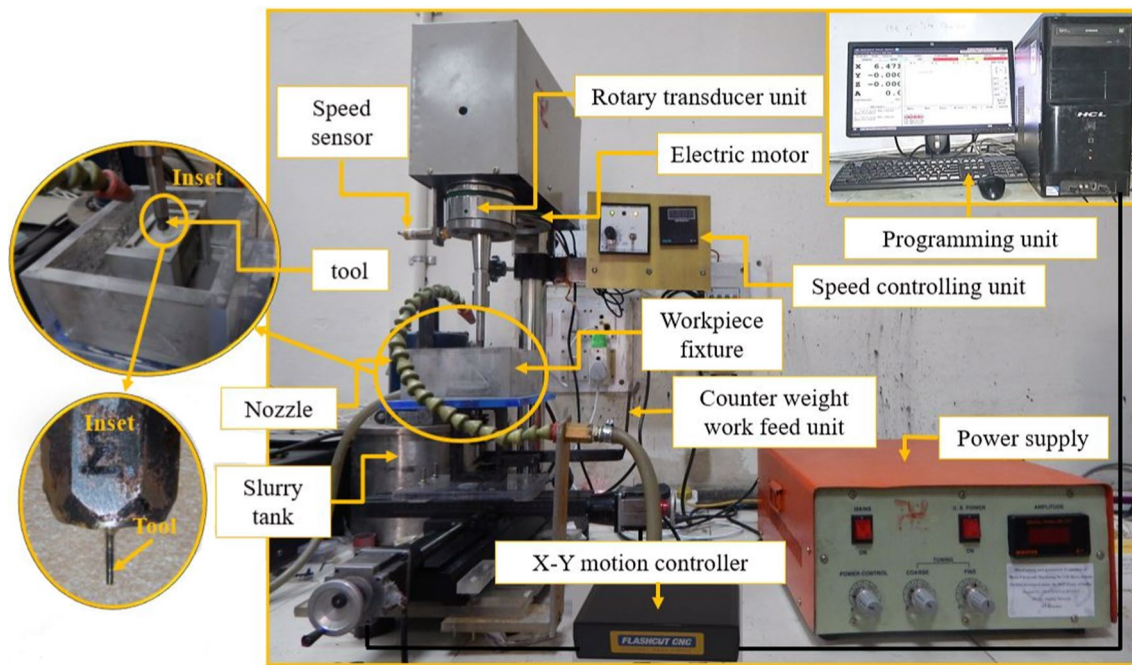
Fig. 1 Developed RMUSM process facility [29]

Table 1 Properties of tool materials

Properties	Tool material	
	SS-304	WC
Compressive strength (MPa)	205–310	3350–6833
Fracture toughness (MPa m$^{1/2}$)	119–228	2–3.8
Vickers hardness (HV)	200	1600
Tensile strength (MPa)	510–620	370–530
Density (g/cm3)	7.85–8.06	15.25–15.88
Crystal structure	BCC	Hexagonal
Speed of sound (m/s)	5800	6220

Table 2 Experimental settings used for experimentation

Experimental details	
Frequency (kHz)	21 ± 1
Peak-to-peak amplitude (μm)	12
Tool rotation speed (rpm)	100–600
Work feed rate (mm/min)	10–30
Power rating (%)	20–60
Slurry concentration (%)	10–30
Abrasive size (mesh)	#1200
Static load (g)	45
Abrasive material	Silicon carbide
Tool material	Tungsten carbide, stainless steel-304
Tool size (μm)	Ø 600
Work material	Borosilicate crown (BK7) glass
Liquid medium used	Water

stage. A counterbalanced tool feed mechanism was used to control the machining gap [30]. Tungsten carbide (WC) and stainless steel of grade 304 (SS-304) were selected as tool materials. The properties of both the tool materials are tabulated in Table 1. Silicon carbide (#1200 mesh size) and tap water were selected as abrasive material and liquid medium for slurry, respectively. The flow of abrasive slurry in between the tool and workpiece was kept constant throughout the experimentation. The performance of RT-MUSM process is influenced by tool rotation speed, work feed rate, power rating and slurry concentration [26, 27, 29, 31, 32]. Therefore, the variable input process parameters selected in this study were tool rotation speed, feed rate, power rating and concentration. The performance of RT-MUSM process was evaluated in terms of MRR, DOC and WOC. The working range (as tabulated in Table 2) of all

the input variable parameters was selected after reviewing the literature and subsequent preliminary experimentation. The experiments were performed as per the parametric conditions given in Table 2 using one-factor-at-time (OFAT) approach. During layer-by-layer machining approach, four passes were given to the workpiece (forward and backward alternatively). During each pass, the workpiece was moved at a distance of 10 mm in X-direction. After the completion of every pass, the tool automatically feeds in the Z-direction using counter-balanced tool feeding system. After each experiment, the samples were cleaned in ultrasonic bath

using ultrasonic cleaner and dried in hot air. Subsequently, all the measurements were taken. An optical microscope (Dewinter Material Plus: DMI Premium) was used to measure the depth and width of machined microchannels. The WOC was calculated by subtracting the tool diameter from the width of the machined microchannels (Fig. 2a) [33]. The MRR was calculated by dividing the weight difference of the workpiece before and after machining by machining time [34]. The formulas used for the calculation of WOC and MRR are expressed in Eqs. (1) and (2), respectively. Post machining, tools were also cleaned and dried. The hardness of the machining face of tools before and after machining was measured with the help of microhardness tester (Make: Omnitech-S. Auto). A constant load of 0.5 N was applied with dwell time of 10 s while measuring the hardness. The images of the tool were captured using stereo microscope (Make: NIKON SMZ-745T). To examine the machined profile, the workpiece was cut along the axis A–A′ (Fig. 2b). The front and top view of the cross section of microchannel are shown schematically in Fig. 2c. Subsequently, the profile was captured and characterized using stereo-microscope.

$$WOC(\mu m) = (W_c - D_t) \qquad (1)$$

where, WOC, W_c and D_t are the width over cut, width of channel and tool diameter, respectively.

$$MRR(mg/min) = \frac{(W_i - W_f)}{T_m} \qquad (2)$$

where, MRR, W_i, W_f and T_m are the material removal rate, initial weight, final weight of workpiece and machining time, respectively.

3 Wear mechanism of soft/ductile and hard tool materials in RT-MUSM

In order to investigate the wear mechanism of both soft/ductile and hard tool materials in RT-MUSM process, experiments were conducted by using both the tool materials (i.e., SS-304 and WC). During the experiments, the machining time was varied from 1 to 5 min and other parameters were kept at their respective constant values (i.e., Tool rotation speed = 300 rpm, feed rate = 15 mm/min, power rating = 30%, concentration = 10% and static load 45 g). After each experiment, tool images (front and bottom view) were captured using stereo microscope. The microscopic images of the tools after machining are presented in Fig. 3. On the basis of the microscopic images, the wear mechanism of SS-304 and WC tool material was explained. From the microscopic images of the tool shown in Fig. 3a-2, a-3, plastic deformation can be clearly seen on the bottom face of SS-304 tool. Whereas, no such effect was observed on the bottom face of WC tool (Fig. 3b-2, b-3). This can be attributed with the fact that in RT-MUSM process, when the tool impacts on the abrasives, the abrasives absorbs kinetic energy and release this energy on the work surface in the form of impact. As a result of that microcracks generate, propagate and finally microchipping takes place by the continuous hitting of abrasives on the work surface. During machining with RT-MUSM process, the tool also suffers the same impacts as the work material. Due to which compressive stresses are generated on the tool bottom surface. By the continuous impact of abrasives, compression of tool bottom face takes place. Consequently, plastic deformation starts to take place in the tool bottom surface (Fig. 4a). This deformation results in the flow of tool material in an upward direction around the periphery of the tool leading to an increase in tool bottom face diameter (Fig. 3a-3). The plastic deformation and increased diameter of tool bottom face are evidenced in Fig. 3p-2, p-3. The
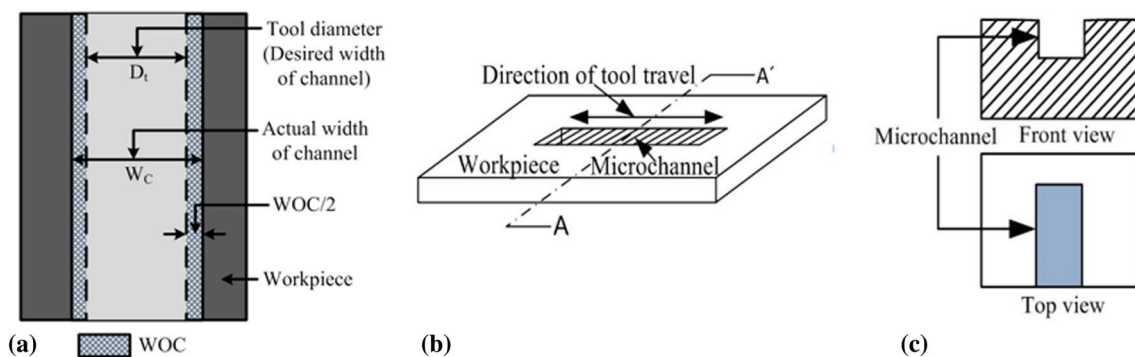

Fig. 2 Schematic representation showing **a** WOC, **b** isometric view of machined microchannel, **c** front and top view of cross section of microchannel
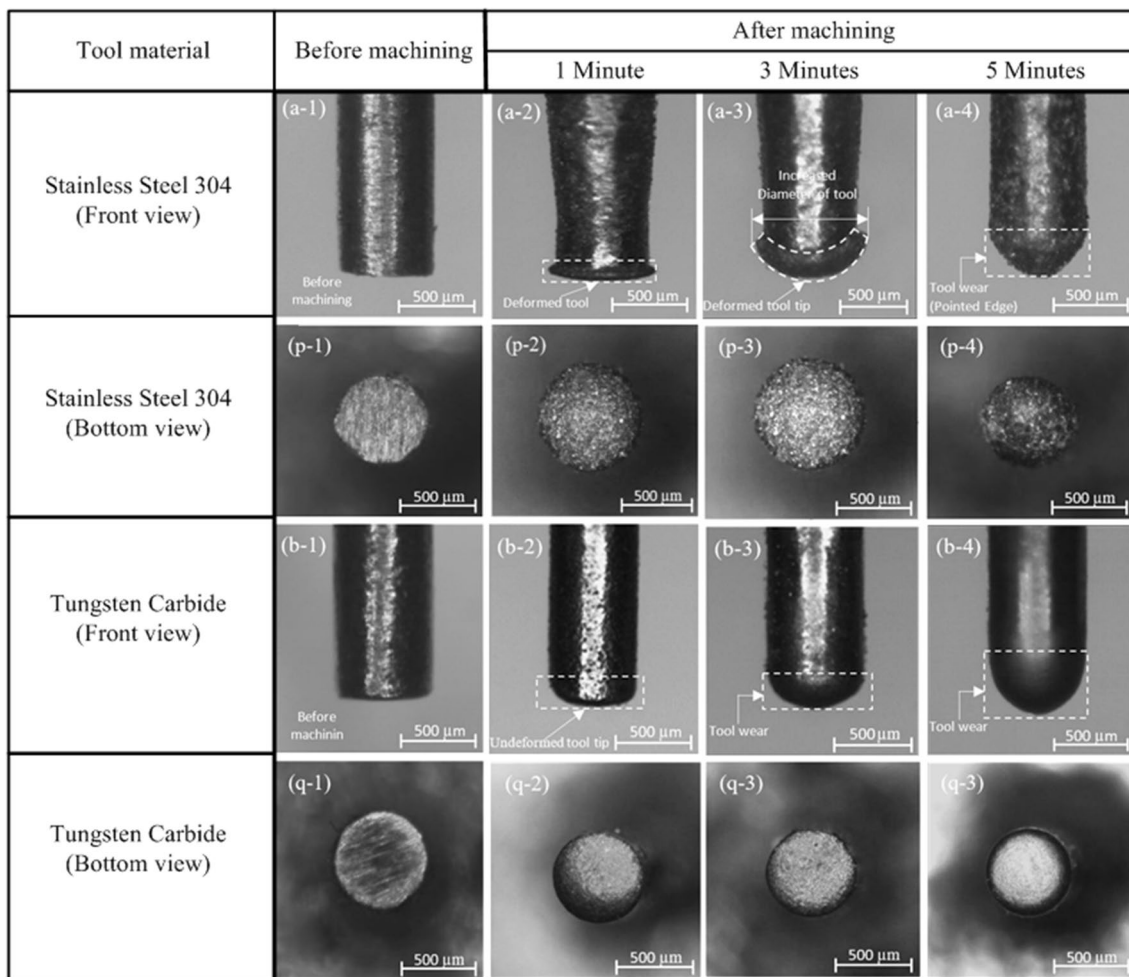
Fig. 3 Tool images before and after machining [experimental conditions: rotation speed = 300 rpm, feed rate = 15 mm/min, power rating = 40%, concentration = 20%]

Fig. 4 Schematic representation showing **a** plastic deformation, **b** shearing of SS-304 tool material
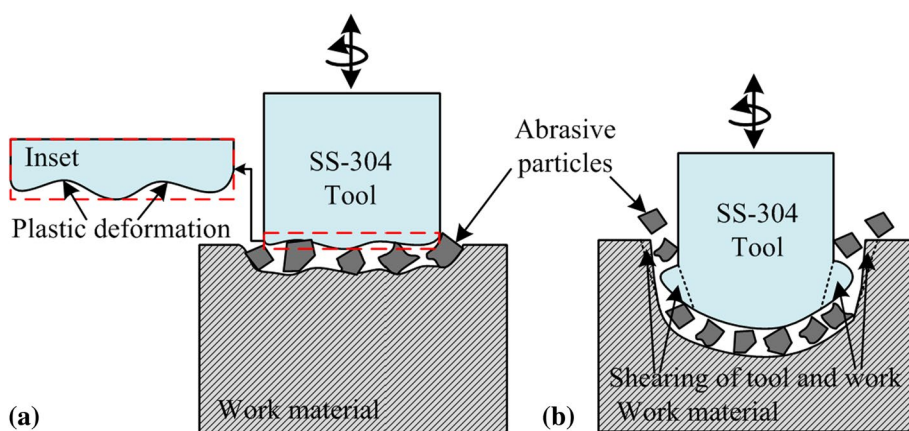
increased tool bottom face diameter in turn results in the increased width of microchannel (Fig. 5b). As the machining continues, this deformation keeps on increasing and as a result of that more and more material accumulates around the periphery of the tool bottom face. Finally, a mushroom-type shape of the tool (as evidenced in Fig. 3a-3) was formed [23]. The mushroom shape of the tool restricts the movement of abrasives from the machining gap (Fig. 4b) due to
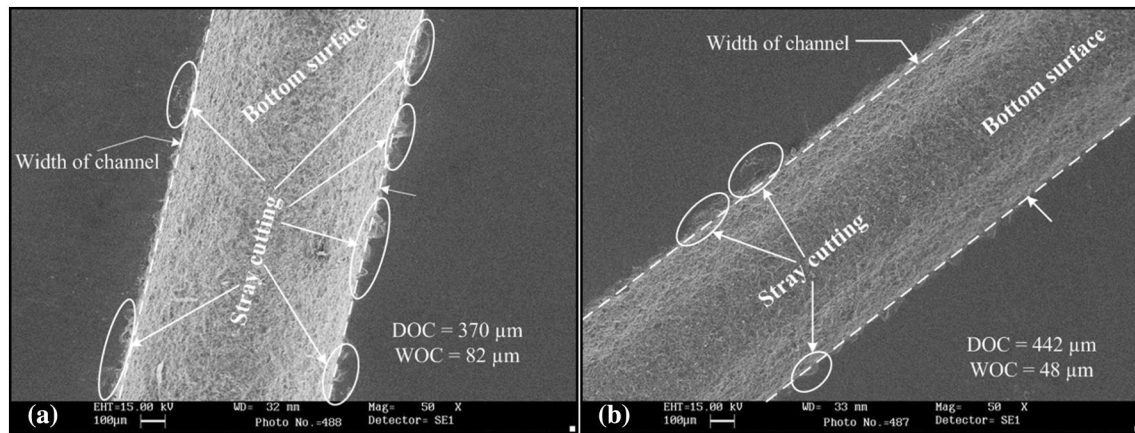
Fig. 5 Machined microchannel using **a** WC tool, **b** SS-304 tool [machining conditions: rotation speed = 400 rpm, feed rate = 15 mm/min, power rating = 40%, concentration = 15% and machining time = 3 min]

which machining rate decreases. Moreover, due to the accumulated unwanted material on the periphery of tool, complete energy is unable to be transferred on the work surface. Consequently, machining rate decreases. On further machining, shearing of accumulated unwanted material on the tool periphery and microchannel wall takes place. The shearing action is schematically presented in Fig. 4b. The shearing of tool and work material takes place due to the abrasion caused by abrasives present in the lateral gap. Consequently, a pointed edge of the tool was obtained (Fig. 3b-4). Whereas, in the case of WC tool material, no compression of tool bottom face was observed (Fig. 3b-2). This can be attributed to high compressive stress of the WC tool. The hardness of WC tool is much higher than SS-304 tool material. Due to high hardness, the WC tool does not deform by the impact of abrasives during entire machining. In case of WC tool, no diametric expansion was observed at tool bottom face (Fig. 3q-2, q-3). As the machining continued, slightly rounded edges of WC tool (i.e., edge rounding wear) were observed after 3 min of machining. Consequently, diameter of the tool bottom face marginally reduced leading to the reduction in WOC of machined microchannel (as evidenced in Fig. 5a). The increased edge rounding wear was observed at continuous machining time of 5 min. The top view of microscopic images of the microchannel machined by using both the materials are presented in Fig. 5a, b, respectively. From Fig. 5a, b, it can be clearly observed that WC tool resulted in the formation of microchannels with lesser WOC (i.e., 48 μm) as well as higher depth (442 μm) as compared to SS-304 tool (WOC = 370 μm and depth = 82 μm). Further, lesser microchipping was observed in the machined microchannel when WC tool was used.

From Fig. 3a-2, a-3, a-4 and b-2, b-3, b-4, it can be clearly seen that in case of RT-MUSM process, no lateral wear was observed on the vertical surface of the tool which indicates that in this process, the tool suffers from longitudinal wear and edge wear only. This is evidenced in the SEM micrograph of tool shown in Fig. 6a, b. The reason behind this was that in RT-MUSM, during exit of the abrasives from the machining gap, the centrifugal force generated by the rotating tool pushes the abrasives toward the wall of machined cavity. Subsequently, these abrasives abraded the side wall of the machined cavity without abrading the vertical surface of the tool. This implies that a two-body abrasion occurs between the abrasives and side wall of machined cavity [27].

4 Results and discussion

4.1 Effect of tool material properties on tool wear, MRR and surface roughness

In RT-MUSM process, the tool material properties (i.e., hardness, impact strength, compressive strength, acoustic property, etc.) play a significant role in tool wear, MRR and quality of machined surface. Tool wear is an intricate phenomenon of micro-USM process which arises from the impact/hammering action of abrasives at ultrasonic frequency. The wear phenomenon of both the tool materials was investigated on the basis of the experiments conducted using the parametric settings given in Table 2. During experimentation, a fresh tool was used for each experiment. After machining, the length and machining face diameter of the tool were measured using stereo microscope. The results obtained are presented in Fig. 7. From Fig. 7a, it can be observed that by increasing the machining time from 1 min to 5 min, the longitudinal wear of both the tools increased almost linearly. The WC tool showed lesser tool wear as compared to the SS-304 tool. The longitudinal wear occurs due to indentation and abrasion caused by the abrasive
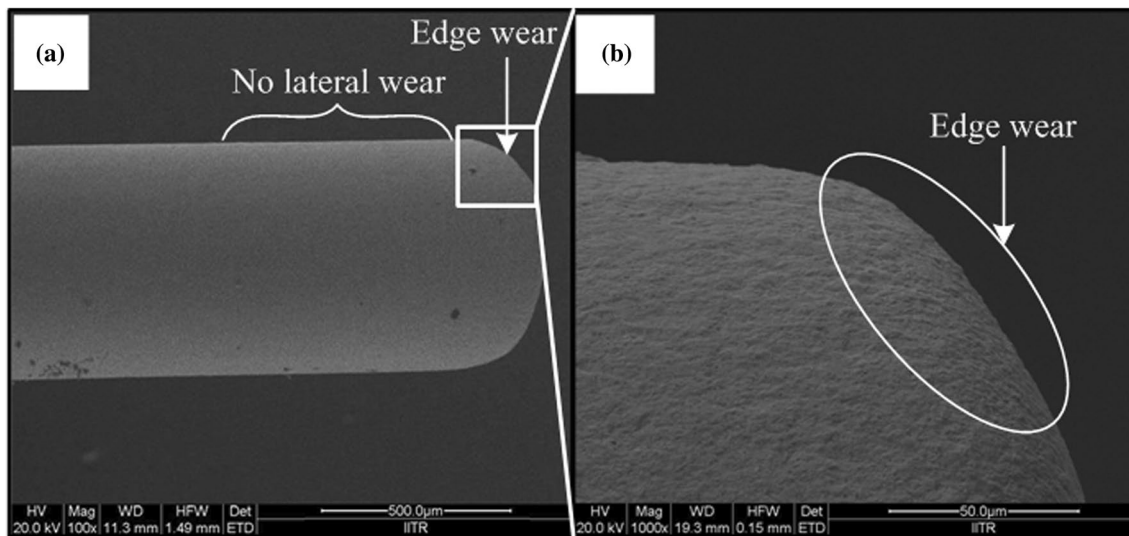
Fig. 6 SEM micrograph of worn out tool showing **a** lateral face, **b** abraded edge of tool
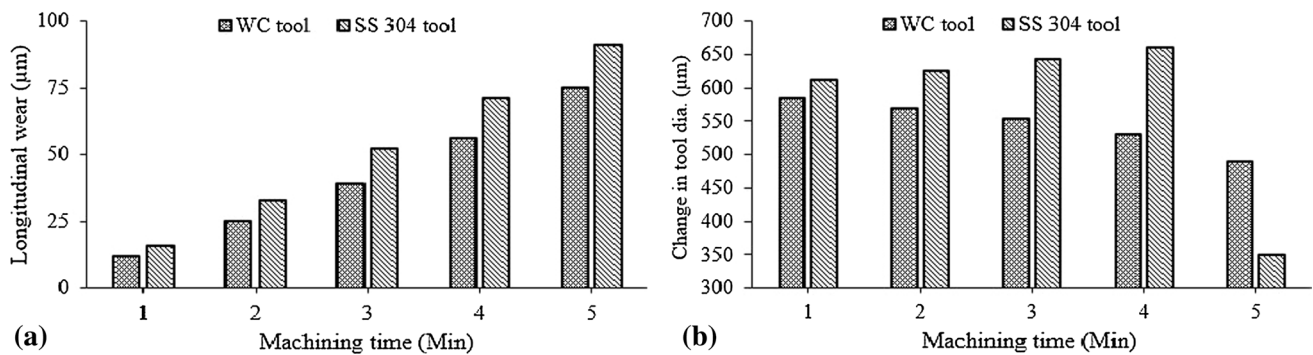

Fig. 7 a Effect of machining time on longitudinal wear, **b** effect of machining time on change in tool diameter

particles. This was attributed to the fact that WC has the higher hardness and compressive strength than the SS-304 tool. The hard surface of WC provided high resistance toward abrasion and indentation leading to lower longitudinal wear. From Fig. 7b, it can be clearly seen that the WC tool face diameter decreased continuously by increasing the machining time. The edge rounding of WC tool face was due to the abrasion only. On the other hand, in case of SS-304 tool, the bottom face diameter increased up to 3 min of machining and after that a sharp decreasing trend was observed. The diametric expansion (i.e., mushroom effect) of the bottom face of SS-304 tool was due to the plastic deformation caused by the repetitive impacts/hammering caused by the abrasive particles. The mushroom effect is evidenced in Fig. 3a-3. Subsequently, due to excessive compressive stress, strain hardening occurred in SS-304 tool leading to an increase in the hardness of the bottom face of tool. From Fig. 8b, it can be observed that even after strain hardening, the hardness of SS-304 tool bottom face was lesser than the

hardness of WC tool. On further machining, the hardened surface layer of the SS-304 dislodged due to abrasion and the diameter of tool suddenly reduced (Fig. 7b). In case of WC tool, no strain hardening phenomenon was observed. The hardness of WC tool remains almost the same. During the entire machining period (i.e., 5 min), the overall diametric reduction in the bottom face of the tools was more when SS-304 tool was used. This was due to the lower hardness of SS-304 than WC which caused greater abrasion in SS-304.

The effect of tool material on MRR is presented in Fig. 8a. It can be seen that WC tool resulted in higher MRR as compared to SS-304 tool throughout machining. The high hardness of WC was responsible for higher MRR. It is believed that the indentation of abrasive particles into the tool face/work surface is inversely proportional to the hardness of tool [21]. Harder surface of WC tool faced lower indentation depth by abrasive particles which led to higher indentation depth into the work surface and thereby, increased the fractured area on the work
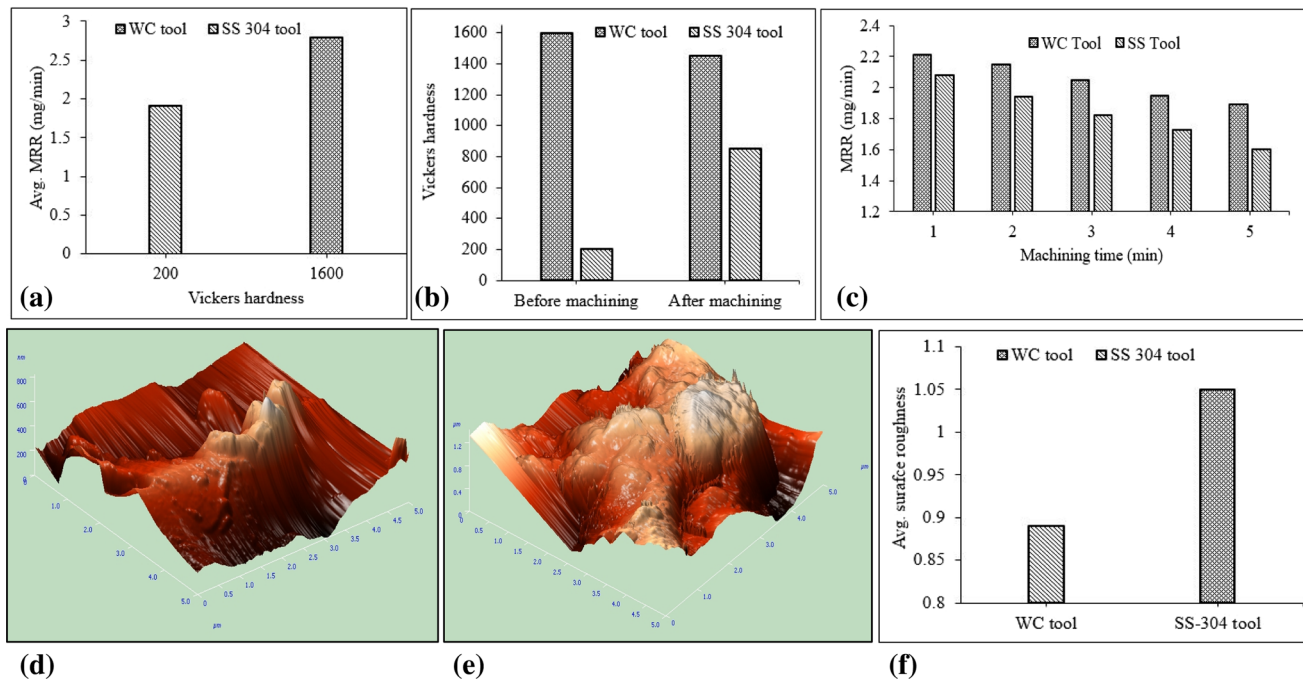
Fig. 8 **a** Effect of hardness on Avg. MRR, **b** hardness before and after machining, **c** machining rate (WC has low rate than SS-tool), **d** machined surface roughness using WC tool, **e** machined surface roughness using SS-304 tool and **f** effect of tool material on surface roughness

surface. Thus, higher MRR was obtained. Further, it can be clearly seen in Table 1 that the acoustic properties of the WC is better than SS-304 tool. This also led to the higher ultrasonic energy transfer by WC tool on the work surface via abrasives. As a result of that higher MRR and low tool wear were obtained by using WC tool material. It was also observed that the machining rate decreased by increasing the machining time using both the tools (Fig. 8c). This may be attributed to the fact that as the machining depth increased, the replenishment of abrasives became difficult which led to an increase in the tool wear. Further, poor slurry replenishment may also lead to the crushing of abrasive particles. Consequently, machining rate decreased. But, this decrease in machining rate was faster in SS-304 as compared to WC tool.

The effect of tool material properties on the machined surface quality was also investigated and presented in Fig. 8d–f. It was observed that the harder tool material (i.e., WC tool) resulted in a smooth machined surface as compared to the softer tool (i.e., SS-304 tool). This was attributed to the higher wear resistance of WC which protected the machining face of WC tool against wear which in turn resulted in finished machined surface. The wear resistance of SS-304 tool is lower than WC due to which rough machined surface was obtained.

4.2 Effect of tool rotation speed

The effect of tool rotation speed on DOC, MRR and WOC is presented in Fig. 9a–c, respectively. It can be observed from Fig. 9a, b that by increasing the rotation speed of tool from 100 rpm to 400 rpm, the DOC and MRR increased by using both the SS-304 and WC tools. After that both started to decrease. Tool rotation exerts centrifugal force on the abrasives in outward direction in the machining zone. The centrifugal force facilitated the abrasives to move out and subsequently, new fresh sharp abrasives entered into the machining area and participated in machining. This led to effective machining and as a result of that DOC and MRR increased. Beyond 400 rpm, the centrifugal force increased significantly and required quantity of abrasives could not get enough time to interact with tool and subsequently on the workpiece. Consequently, DOC and MRR decreased. The effect of tool rotation speed on width overcut is shown in Fig. 9c. While using SS-304 tool, the WOC increased by increasing the tool rotation speed. This can be inferred that by increasing tool rotation speed up to 400 rpm, more number of abrasives interacted with the tool. Due to which the tool bottom surface suffered by more number of impacts/ hammering action which caused plastic deformation of
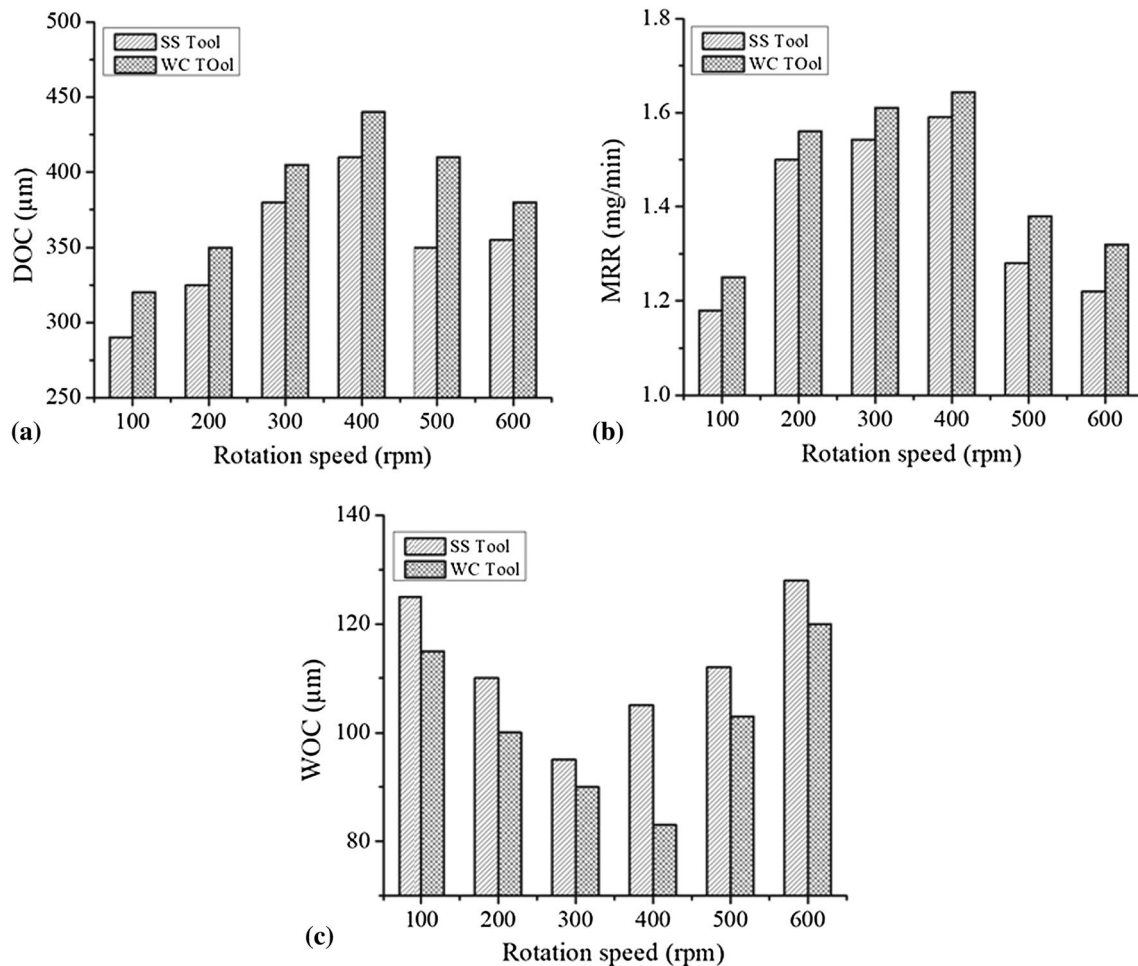
Fig. 9 Effect of rotation speed on **a** DOC, **b** MRR, **c** WOC

SS-304 tool bottom face. Consequently, the diameter of SS-304 tool bottom face increased due to which higher WOC was obtained. Beyond 400 rpm, the tool worn out owing to shearing of unwanted deformed material and hence WOC decreased. In case of WC tool, WOC initially decreased up to 400 rpm of the tool due to the effective replenishment of abrasives from the machining zone. Thus, WOC reduced. Beyond 400 rpm, an increasing trend in WOC was observed. Also, the rotation speed of 400 rpm resulted in best possible form accuracy of the microchannels using both the tools. The cross-sectional view of microchannel obtained at 400 rpm rotation speed is shown in Fig. 13a. At higher rotation speed, tool may come in direct contact with the work material leading to damage of both the tool and work material. Moreover, the lateral vibration may generate in the tool at higher rotation speed which may be responsible for higher WOC.

4.3 Effect of feed rate

In this process, feed rate decides the interaction time between tool, abrasives and work material. The effect of feed rate of work on DOC, MRR and WOC of microchannels is illustrated in Fig. 10a–c, respectively. From Fig. 10a, b, it can be seen that in case of both SS-304 and WC tool, the DOC and MRR initially increased by increasing the feed rate up to 20 mm/min and after that a decreasing trend was observed. This can be explained with the fact that low feed rate increases the interaction time between tool, abrasives and work, but at the same time more abrasives interacted with the tool creating more than one layer of abrasives in the machining gap leading to loss of energy. Thus, lower DOC and MRR were obtained. Whereas, at higher values of feed rate (greater than 20 mm/min), the interaction time was significantly reduced due to which low DOC and MRR
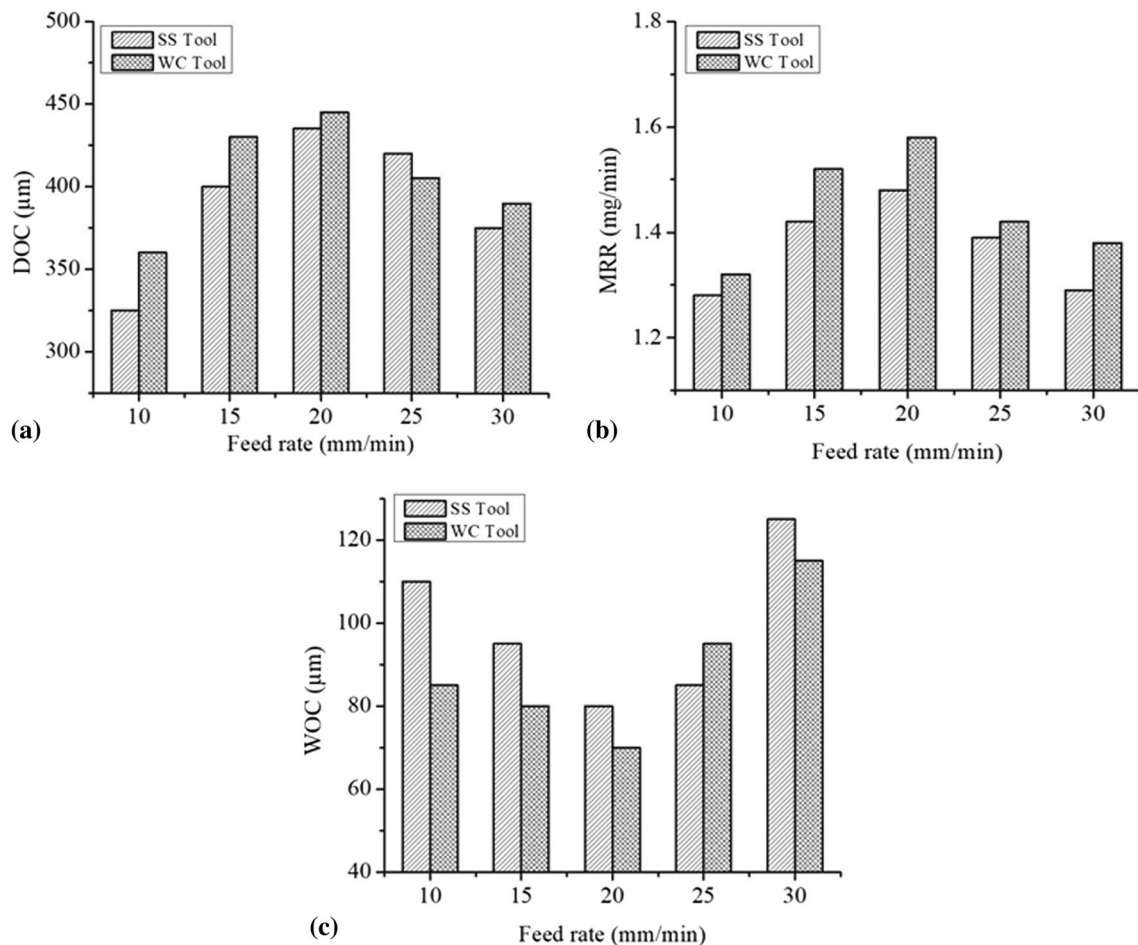
Fig. 10 Effect of feed rate on **a** DOC, **b** MRR, **c** WOC

was observed. At a feed rate of 20 mm/min, uniform machining was observed and as a result of that maximum DOC and MRR were achieved. In case of both the SS-304 and WC tool, the WOC decreased by increasing the feed rate up to 20 mm/min and beyond that it increased (Fig. 10c). At low feed rate (10 mm/min), the excessive plastic deformation increased the tool bottom face diameter which led to an increase in WOC. On increasing the feed rate lesser plastic deformation took place and as a result of that low WOC was obtained. The workpiece feed rate of 20 mm/min also resulted in best possible form accuracy of machined microchannels. The cross-sectional view of microchannel obtained at 20 mm/min feed rate is shown in Fig. 13b.

4.4 Effect of power rating

The power rating is directly related to the amount of energy imparted by the tool to the work surface via abrasive particles. Higher power rating increases the amplitude of vibration due to which the tool transfers more energy to the abrasives in the form of impact. Subsequently, this energy reaches to the work surface via abrasives in the form of impact force. Thus, higher the power rating, higher will be the impact force on work surface and vice versa. The effect of power rating on DOC, MRR and WOC is presented in Fig. 11a–c, respectively. From Fig. 11a and b it can be observed that by increasing the power rating from 20% to 60%, both the DOC and MRR increased continuously in both the SS-304 and WC tool. This can be inferred that on increasing power rating, the abrasives impact on work surface with higher force (energy) due to which depth of crater increased leading to more material removal from work surface. Thus, DOC and MRR increased. On the other hand, the WOC initially increased by increasing the power rating up to 40% and after that a decreasing trend was observed using both the SS and WC tools (Fig. 11c). The higher impact force was responsible for increased WOC up to 40% power rating. After 40% of power rating, the WOC decreased owing to the high tool wear. The best possible form accuracy of microchannel was obtained at 40% of power rating. The cross-sectional view of microchannel obtained at 40% power rating is shown in Fig. 13c. Moreover, at higher
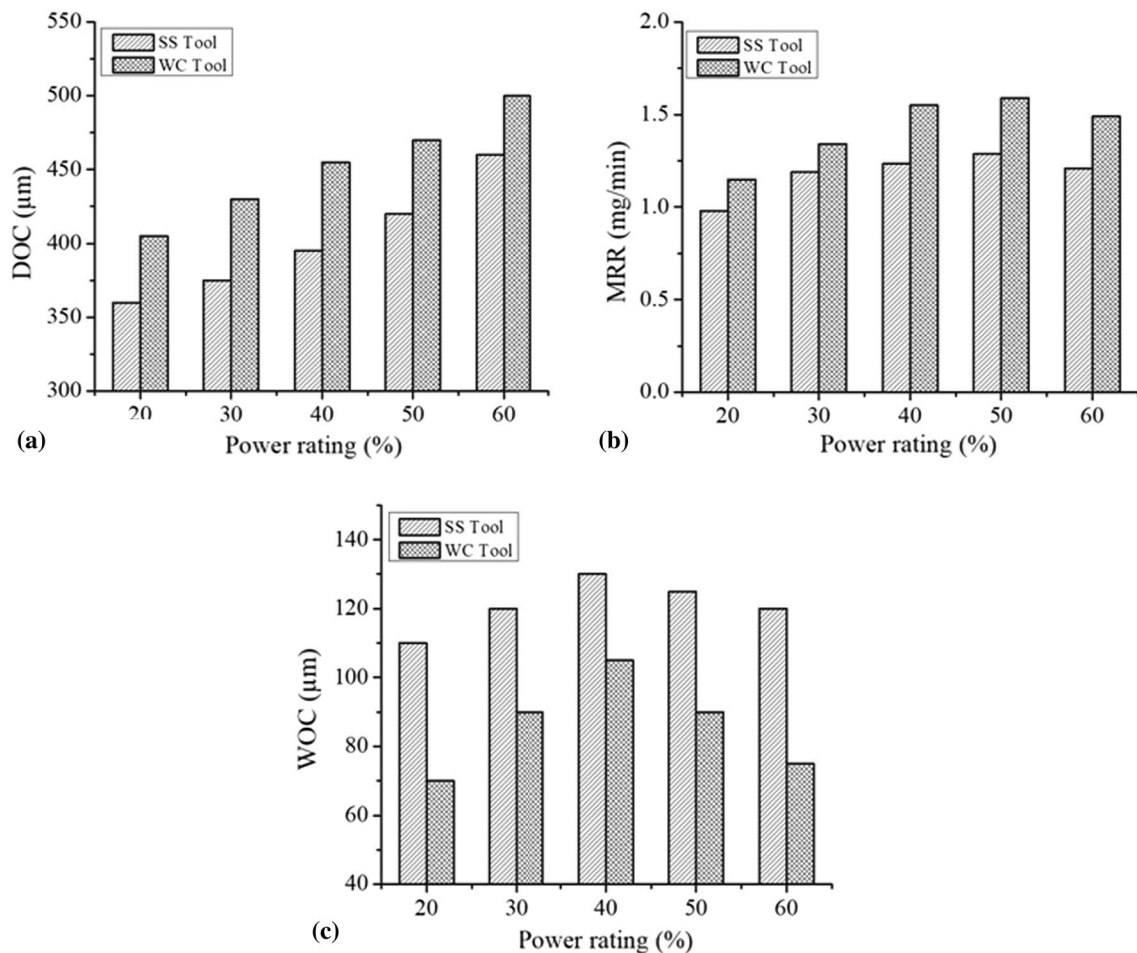
Fig. 11 Effect of power rating on **a** DOC, **b** MRR, **c** WOC

power rating, the crushing of abrasives may be another reason responsible for low DOC, MRR and WOC.

4.5 Effect of slurry concentration

The quantity of abrasives is directly proportional to the concentration of abrasive slurry. The effect of slurry concentration on DOC, MRR and WOC is presented in Fig. 12a–c, respectively. From Fig. 12a, b it can be observed that by increasing the concentration of slurry, the DOC and MRR increased up to 20% of concentration and beyond that a decreasing trend was observed in both the SS-304 and WC tool. The reason can be inferred that the number of abrasives in the machining gap increased by increasing the concentration. Subsequently, the number of impacts on the work surface increased leading to more material removal from work surface. Thus, DOC and MRR increased. On further increasing the concentration beyond 20%, multiple layers of abrasives were stacked over each other. This led to loss of ultrasonic energy. Consequently, both the DOC and MRR decreased. The maximum DOC

and MRR were achieved at 20% of concentration by using both the tools. The WOC was increased continuously by increasing the concentration in the case of WC tool (Fig. 12c). This was due to the reason that two-body abrasion in the lateral gap increased by increasing the concentration. On the other hand in the case of SS-304, the WOC increased up to 20% concentration and after that it started to decrease. The decreasing trend may be due to the high tool wear caused by the shearing of the bottom face periphery. A 20% concentration exhibited in best possible form accuracy of machined microchannel. The cross-sectional view of microchannel obtained at 20% concentration is shown in Fig. 13d.

On the basis of above discussion, it can be concluded that in RT-MUSM process, the performance of WC was superior over SS-304 in terms of DOC, MRR and WOC. Also, the microchannels obtained by using WC tool had better form accuracy. Therefore, WC can be suggested as a better tool material for RT-MUSM process. Further, in order to obtain maximum DOC, MRR and minimum WOC, optimization of RT-MUSM process parameters is necessary. In order to
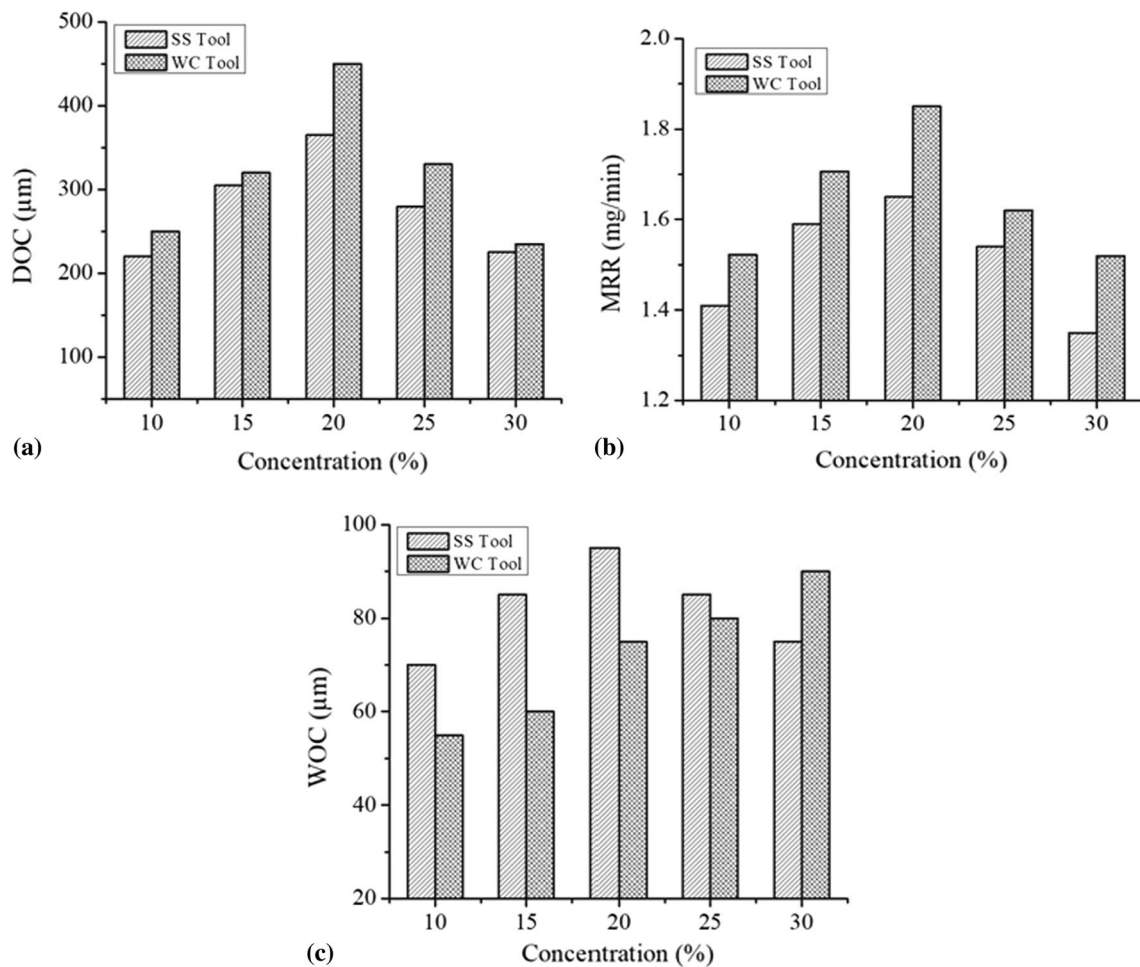
Fig. 12 Effect of concentration on **a** DOC, **b** MRR, **c** WOC

accomplish this objective, the RT-MUSM process is optimized and discussed subsequently.

5 Multi-response optimization of RT-MUSM process with WC tool

The optimization of RT-MUSM process was carried out to determine the input parametric settings that give maximum DOC, MRR and minimum WOC simultaneously. A desirability function approach postulated by Harrington and later revitalized by Derringer and Suich was used to accomplish this objective [35, 36]. This approach is commonly used to optimize the multiple output responses simultaneously [37–41]. In this approach, each of the response variable y_i is normalized to a desirability value d_i which lies in between 0 and 1. The value of d_i depends upon the "desirability" of the corresponding response. The value of d_i increases/decreases with an increase/decrease in response's desirability. The value of $d_i = 0$ shows the undesirable response. On the other hand, if

the value of $d_i = 1$, it shows completely desired response. The following equations are used to express the individual desirabilities as per the desired response (i.e., "higher the better" or "lower the better").

For "higher the better"

$$d_i = \begin{cases} 0 & y_i \leq y_{\min} \\ \left[\dfrac{y_i - y_{\max}}{y_{\max} - y_{\min}}\right]^r & y_{\min} < y_i < y_{\max} \\ 1 & y_i \geq y_{\max} \end{cases} \tag{3}$$

For "lower the better"

$$d_i = \begin{cases} 1 & y_i \leq y_{\min} \\ \left[\dfrac{y_{\max} - y_i}{y_{\max} - y_{\min}}\right]^r & y_{\min} < y_i < y_{\max} \\ 0 & y_i \geq y_{\max} \end{cases} \tag{4}$$

where, $y_{\max}$ and $y_{\min}$ represents the maximum and minimum value of y_i. The value of r decides the shape of desirability
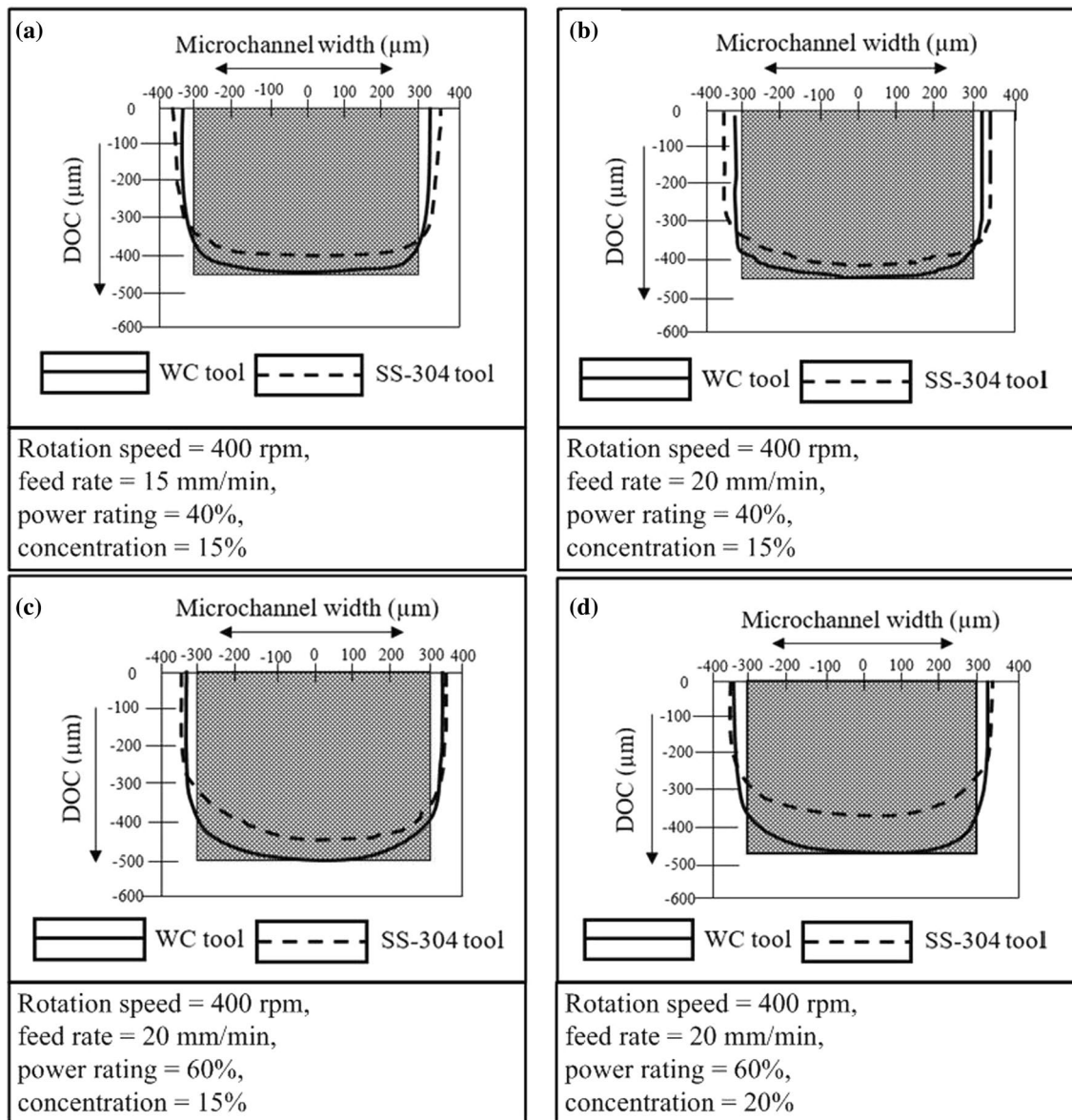
Fig. 13 Cross-sectional profiles of microchannels

function and its value ranges from 0.1 to 10. After determining the value of d_i, overall desirability (d) is calculated using Eq. (5) by taking the geometrical mean of all individual desirability.

$$d = \left(d_1 \times d_2 \times d_3 \cdots \times d_k\right)^{\frac{1}{k}} \quad (5)$$

where, k is the number of responses.

The desirability approach was applied using a Minitab-17 software. For DOC and MRR, "higher the better" and for WOC "lower the better" criteria were applied. During optimization, the goal for DOC and MRR was set to maximize, whereas for WOC, the goal was set to minimize. The goals for input variable were set to "in

Table 3 Process parameters range for DOC, MRR and WOC

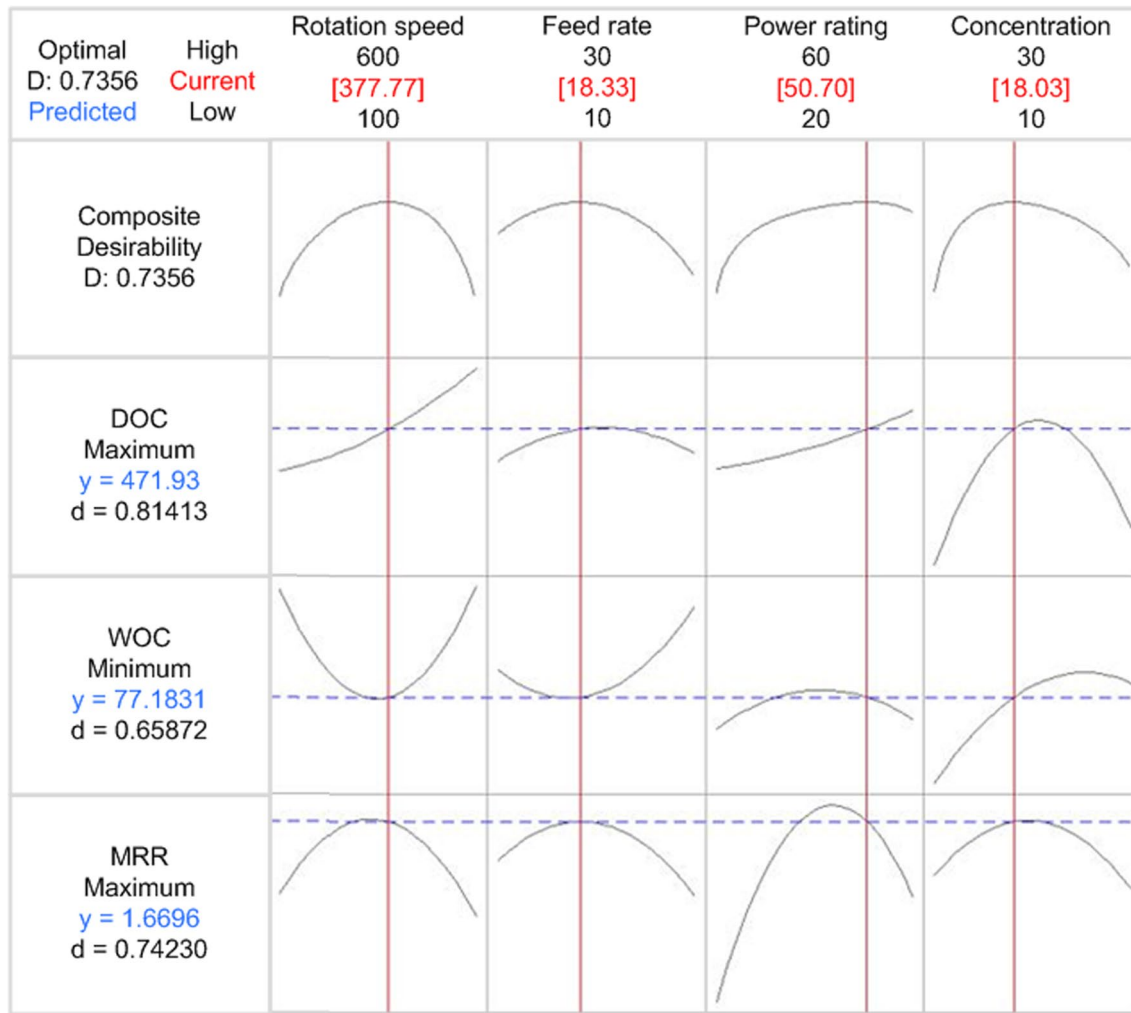| Input parameters	Goal	Constraint limits	
		Lower	Upper
Rotation speed (rpm)	In range	100	600
Work feed rate (mm/min)	In range	10	30
Power rating (%)	In range	20	60
Slurry concentration (%)	In range	10	30
Output parameters	Goal	Weightage	
DOC (µm)	To maximize	1	
MRR (mg/min)	To maximize		
WOC (µm)	To minimize		

Fig. 14 Optimization plot

range". The upper and lower values of input parameters are given in Table 3. Since, both productivity (i.e., higher MRR and DOC) and accuracy (lower WOC) are equally important, and therefore, equal weightage was given to all the response variables. The optimized results for all the desired responses are shown in Fig. 14. It can be seen in Fig. 14 that the parametric conditions of rotation speed = 377.77 rpm, feed rate = 18.33 mm/min, power rating = 50.70% and slurry concentration = 18% with desirability of 0.7356 exhibited in maximum DOC, MRR and minimum WOC of 472 μm, 1.66 mg/min and 77 μm, respectively.

Table 4 Results of confirmation experiments

Parametric conditions	Exp. No.	Responses						
		MRR (mg/min)	WOC (μm)	DOC (μm)	Average MRR (mg/min)	Average DOC (μm)	Average WOC (μm)	Average error (%)
Rotation speed = 377 rpm, feed rate = 18.3 mm/min, power rating = 50%, concentration = 18%	1	1.65	68	485	1.76	487	70	7
	2	1.68	64	480				
	3	1.74	78	495				
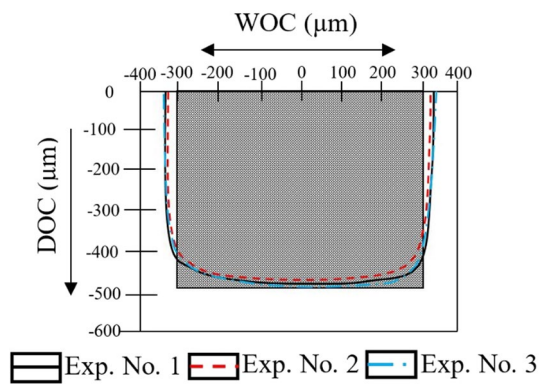
Fig. 15 Cross section view of microchannels obtained at optimal parametric settings

After obtaining the optimal parametric condition for maximum DOC, MRR and minimum WOC, confirmation tests were performed to validate the optimal settings. The confirmation tests were repeated thrice, and the mean value of DOC, MRR and WOC were considered. The results are tabulated in Table 4. Table 4 clearly indicates that the results were very close to each other with an average error of 7%. The cross-sectional view of microchannels obtained at optimal parametric combinations is shown in Fig. 15.

6 Conclusions

In this investigation, the wear mechanism of soft/ductile and hard tool materials used in RT-MUSM process is addressed. The effect of tool material properties on tool wear, MRR, DOC and WOC was investigated to evaluate the performance of RT-MUSM process. Further, the RT-MUSM process parameters, viz. tool rotation speed, work feed rate, power rating and slurry concentration were also investigated comprehensively. Additionally, the RT-MUSM process was optimized to achieve maximum MRR, DOC and minimum WOC simultaneously. The conclusion drawn from the current study can be summarized as follows:

- The SS-304 tool suffered from plastic deformation and strain hardening which caused higher longitudinal wear, edge wear and poor dimensional accuracy of microchannels as compared to the WC tool in which no strain hardening was observed.
- The hardness, impact strength and acoustic property of tool material significantly affected the performance of RT-MUSM process.
- Both very high and low tool rotation speed, work feed rate and slurry concentration diminished the performance of RT-MUSM process by decreasing the MRR, DOC and

increasing WOC of machined microchannels using both SS-304 and WC tool materials.
- An increase in power rating increased the MRR and DOC but at the same time dimensional accuracy of machined microchannel was found to be decreased.
- Owing to superior properties, the performance of WC tool material was found to be better in terms of higher MRR, DOC, lower WOC and better form accuracy of machined microchannels as compared to SS-304.
- The parametric conditions of tool rotation speed = 377.77 rpm, feed rate = 18.33 mm/min, power rating = 50.70% and concentration = 18.03% were found to be optimal and resulted in maximum MRR = 1.66 mg/min, DOC = 471.93 μm and minimum WOC = 77 μm in RT-MUSM process with WC tool material.

References

1. Guruparan GK, Sathish M (2006) Design and fabrication of micro channels for MEMS applications. Synth React Inorg Met Org Chem 36:185–191
2. Fan Y, Luo L (2008) Recent applications of advances in microchannel heat exchangers and multiscale design optimization. Heat Transf Eng 29(5):461–474
3. Saranya S, Sankar AR (2018) Fabrication of precise microchannels using a side-insulated tool in a spark assisted chemical engraving process. Mater Manuf Process 33(13):1422–1428
4. Rattan N, Mulik RS (2017) Experimental investigations and multiresponse optimization of silicon dioxide (Quartz) machining in magnetic field assisted TW-ECSM process. Silicon 9:663–673
5. Thoe TB, Aspinwall DK, Wise MLH (1998) Review on ultrasonic machining. Int J Mach Tools Manuf 38:239–255
6. Hu X (2007) Mechanism, characteristics and modeling of micro ultrasonic machining, Ph.D. thesis, University of Nebraska-Lincoln
7. Benedict GF (1981) Non-traditional manufacturing processes. Marcel Dekker Inc., New York
8. Maurotto A, Muhammad R, Roy A, Babitsky VI, Silberschmidt VV (2012) Comparing machinability of Ti-15-3-3-3 and Ni-625 alloys in UAT. Proc CIRP 1:330–335
9. Riaz M (2013) Hot ultrasonically assisted turning of Ti–15V3Al-3Cr3Sn: experimental and numerical analysis, Ph.D. thesis Loughborough University, Leicestershire
10. Khajehzadeh M, Akhlaghi M, Razfar MR (2014) Finite element simulation and experimental investigation of tool temperature during ultrasonically assisted turning of aerospace aluminum using multicoated carbide inserts. Int J Adv Manuf Technol 75(5–8):1163–1175
11. Kumar MN, Subbu SK, Krishna PV, Venugopal A (2014) Vibration assisted conventional and advanced machining: a review. Procedia Eng 97:1577–1586
12. Maurotto A, Wickramarachchi CT (2016) Experimental investigations on effects of frequency in ultrasonically-assisted end-milling of AISI 316L: a feasibility study. Ultrasonics 65:113–120

13. Zheng K, Li Z, Liao W, Xiao X (2017) Friction and wear performance on ultrasonic vibration assisted grinding dental zirconia ceramics against natural tooth. J Braz Soc Mech Sci Eng 39(3):833–843

14. Sofuoglu MA, Çakır FH, Gürgen S, Orak S, Kuşhan MC (2018) Experimental investigation of machining characteristics and chatter stability for Hastelloy-X with ultrasonic and hot turning. Int J Adv Manuf Technol 95(1–4):83–97

15. Sofuoğlu MA, Çakır FH, Gürgen S, Orak S, Kuşhan MC (2018) Numerical investigation of hot ultrasonic assisted turning of aviation alloys. J Braz Soc Mech Sci Eng 40(3):122

16. Moghaddas MA, Short MA, Wiley NR, Yi AY, Graff KF (2018) Performance of an ultrasonic-assisted drilling module. Int J Adv Manuf Technol 94(9–12):3019–3028

17. Liu J, Jiang X, Han X, Gao Z, Zhang D (2019) Effects of rotary ultrasonic elliptical machining for side milling on the surface integrity of Ti–6Al–4V. Int J Adv Manuf Technol 101(5–8):1451–1465

18. Cheema MS (2015) An ultrasonic micromachining approach to fabricate microchannels on glass. Ph.D. Thesis, IIT Roorkee

19. Yu Z, Ma C, An C, Li J, Guo D (2012) Prediction of tool wear in micro USM. CIRP Ann Manuf Technol 61:227–230

20. Jain V, Sharma AK, Kumar P (2011) Investigations on tool wear in micro ultrasonic machining. Appl Mech Mater 110–116:1561–1566

21. Komaraiah M, Reddy PN (1993) Relative performance of tool materials in ultrasonic machining. Wear 161:1–10

22. Adithan M, Venkatesh VC (1975) Tool wear mechanisms in ultrasonic drilling. Wear 34:449–453

23. Cheema MS, Dvivedi A, Sharma AK (2015) Tool wear studies in fabrication of microchannels in ultrasonic micromachining. Ultrasonics 57:57–64

24. Wang J, Shimada K, Mizutani M, Kuriyagawa T (2018) Tool wear mechanism and its relation to material removal in ultrasonic machining. Wear 394:96–108

25. Yu Z, Hu X, Rajurkar KP (2006) Influence of debris accumulation on material removal and surface roughness in micro ultrasonic machining of silicon. CIRP Ann Manuf Technol 55:201–204

26. Kumar S, Dvivedi A (2019) On machining of hard and brittle materials using rotary tool micro-ultrasonic drilling process. Mater Manuf Process 34(7):736–748

27. Kumar S, Dvivedi A (2018) Fabrication of microchannels using rotary tool micro-USM: an experimental investigation on tool wear reduction and form accuracy improvement. J Manuf Process 32:802–815

28. Pal RK, Garg H, Sarepaka RGV, Karar V (2016) Experimental investigation of material removal and surface roughness during optical glass polishing. Mater Manuf Process 31:1613–1620

29. Kumar S, Dvivedi A (2019) On effect of tool rotation on performance of rotary tool micro-ultrasonic machining. Mater Manuf Process 34(5):476–486

30. Pandey PC, Shan HS (1980) Modern machining processes. Tata McGraw-Hill, New Delhi

31. Kumar S, Dvivedi A (2017) Experimental investigation on drilling of borosilicate glass using micro-USM with and without tool rotation: a comparative study. Int J Addit Subtr Mater Manuf 1:213–222

32. Kumar S, Dvivedi A, Kumar P (2017) On tool wear in rotary tool micro-ultrasonic machining. In: Proceedings of the 3rd Pan American materials congress, Springer, Cham, pp 75–82

33. Sreehari D, Sharma AK (2018) On form accuracy and surface roughness in micro-ultrasonic machining of silicon microchannels. Precis Eng 53:300–309

34. Yadav RN, Yadava V (2014) Slotted-electrical discharge diamond cut-off grinding of Al/SiC/B4C hybrid metal matrix composite. J Mech Sci Technol 28(1):309–316

35. Harrington EC (1965) The desirability function. Ind Qual. Control 21(10):494–498

36. Derringer G, Suich R (1980) Simultaneous optimization of several response variables. J Qual Technol 12:214–219

37. Sharma V, Kumar V (2016) Multi-objective optimization of laser curve cutting of aluminium metal matrix composites using desirability function approach. J Braz Soc Mech Sci Eng 38:1221–1238

38. Kumar V, Singh H (2018) Machining optimization in rotary ultrasonic drilling of BK-7 through response surface methodology using desirability approach. J Braz Soc Mech Sci Eng 40(2):83

39. Singh RP, Singhal S (2017) Investigation of machining characteristics in rotary ultrasonic machining of alumina ceramics. Mater Manuf Process 32(3):309–3026

40. Kumar A, Kumar V, Kumar J (2015) Semi-empirical model on MRR and overcut in WEDM process of pure titanium using multi-objective desirability approach. J Braz Soc Mech Sci Eng 37:689–721

41. Popli D, Gupta M (2018) Experimental investigation of tool wear and machining rate in rotary ultrasonic machining of nickel alloy. Mach Sci Technol 22(3):427–453